Inlet Flow Effects in Micro-channels in the Laminar and Transitional Regimes on Single-Phase Heat Transfer Coefficients and Friction Factors

Jaco Dirker[*], Josua P. Meyer[**], Darshik V. Garach,

Department of Mechanical and Aeronautical Engineering, University of Pretoria, Pretoria, Private Bag X20, Hatfield 0028, South Africa.

**Corresponding Author:*

Email Address: jaco.dirker@up.ac.za

Phone: +27 (0)12 420 2465

***Alternative Corresponding Author:*

Email Address: josua.meyer@up.ac.za

Phone +27 (0)12 420 3104

ABSTRACT

An experimental investigation of heat transfer and pressure drop in rectangular micro-channels was conducted for water in the laminar and transitional regimes for three different inlet configurations. The inlet types under consideration were the sudden contraction, bellmouth, and swirl inlet types, and hydraulic diameters of 0.57 mm, 0.85 mm, and 1.05 mm were covered. It was found that the critical Reynolds number and the transitional behaviour in terms of heat transfer coefficients and friction factors were influences significantly by the inlet type. For the sudden contraction inlet type, which were investigated for both adiabatic, as well as diabatic cases, adiabatic friction factors were predicted well by the laminar Shah and London correlation, while diabatic friction factors were decreased with an increase in wall heat flux. The sudden contraction inlet critical Reynolds numbers were found to be between 1 800 and 2 000 for adiabatic cases, while for diabatic cases the transition regime commenced at a Reynolds number of about 2 000. The bellmouth and swirl inlet types were investigated for diabatic cases only with swirl inlet tests limited to the 1.05 mm channel. Laminar

friction factors were approximately similar to those of the sudden contraction inlet type, however, after the commencement of transition both inlet types exhibited higher friction factors than the sudden contraction inlet. Minor transition occurred as early as at Reynolds numbers of 1 200 and 800 for the bellmouth and swirl inlet types respectively while major transition occurred at Reynolds numbers of approximately 1 800 and 1 500 respectively. Critical Reynolds numbers were found not be significantly influenced by the channel to diameter to length ratio considered in this study. Laminar Nusselt numbers were predicted well by conventional macro-channel thermal entry correlations. The swirl inlet type exhibited the highest friction factors and Nusselt numbers in the transitional regime followed by the bellmouth inlet type. During transition while compared with the sudden contraction inlet, both the bellmouth and swirl inlet types exhibited larger enhancement in heat transfer than increases in the friction factor penalty. Based on the experimental data obtained in this study, a set of correlations were developed which describes the relation between the friction factor and Colburn *j*-factor. Depending on the inlet type, the correlations predicted between 94% and 100% of the results to within 10% of the experimental measurements.

Keywords: micro-channels, laminar, transitional, inlet flow effects, heat transfer coefficient, friction factor

Nomenclature

a	correlation constant
A_s	channel wall surface area, m^2
b	correlation constant
C_p	specific heat, J/kgK
D	diameter, m
eb	energy balance, %
f	Darcy-Weisbach friction factor
$\bar{h}$	average heat transfer coefficient, W/m^2K

$\bar{I}$	average electric current input, A
j	Colburn *j*-factor
k	thermal conductivity, W/mK
L	channel length, m
L^+	non dimensional channel length
M	axial conduction factor
m	viscosity ratio exponent
$\dot{m}$	mass flow rate, kg/s
$\overline{Nu}$	average Nusselt number
n	thermocouple node number
ΔP	differential pressure, Pa
P	Channel Perimeter, m
Pr	Prandtl number
$\bar{\dot{Q}}$	average heat transfer rate, W
Re	Reynolds number
$\bar{T}$	average temperature, °C
v	average velocity, m/s
$\bar{V}$	average voltage input, V
W	Width, m

Greek Symbols

ε	relative roughness
ρ	density, kg/m^3

Subscripts

b	bulk fluid
$base$	base block
Bl	Blasius equation
f	fluid
Gn	Gnielinski correlation
h	hydraulic
$heater$	heater
i	inner
in	inlet
lam	laminar
$meas$	measured
MY	Muzychka and Yovanovich correlation
$node$	thermocouple node location
o	outer
out	outlet
p	pressure
$pred$	predicted
s	solid
SL	Shah and London correlation
w	wall
$water$	water
$wetted$	wetted

1 Introduction

The pressure drop and heat transfer characteristics of micro channels are important to thermal design engineers in, for instance, the electronics cooling industry. Knowledge of the performance of micro channels in the laminar, transitional and turbulent flow regimes are vital to ensure thermally effective and energy efficient cooling systems. Since the pioneering work of Tuckerman and Pease [1] that demonstrated that the use of micro-channels allowed for increased heat flux level to be sustained, micro-channels have been an active topic of investigation. Tuckerman and Pease who considered multiple rectangular channels in fused silica using water as coolant reported that their thermal resistances were predicted well by convention theory. Subsequent investigations by others followed, and a range of contradicting results were published in terms of friction factor and Nusselt number behaviour as compared to conventional macro-channels behaviour.

Some of these studies [1–18] are summarised in Table 1 and reference is made to the fluid used, cross-sectional channel shape, inlet type, channel material, whether a single channel or multiple parallel channels were investigated, the applied thermal boundary, diameter range considered, the relative roughness of the channel wall, the reported critical Reynolds number and whether conventional macro-channel theory over predicted (>), under predicted (<), or correctly predicted (=) the measured friction factor and Nusselt number. It could be noted that a wide range of critical Reynolds numbers were reported and that there are inconsistencies amongst the reported results for macro channel conformance.

These inconsistencies have spurred on even more research to determine what the underlining cause is of the apparent deviation from macro-scale heat transfer and friction factor behaviour. More resent results indicate that micro-channel behaviour does in fact agree to a better extent with that of macro channels. A number of studies found that many of the inconsistencies could be attributed to the challenges being faced with the accurate measurement of, amongst others, the wall temperature [19], and the bulk fluid temperature [20] used to determine the friction factors and heat transfer coefficients. The presence of axial wall heat conduction has also been an issue which could affect the

accuracy with which the average bulk fluid temperature is determined, which in turn will directly affect the calculated Nusselt number values [21].

Sometimes, however, investigations are conducted for case-specific applications, such as for instance with Steinke and Kandlikar [11], and Hrnjak and Tu [12], who considered multiport micro channel systems. Though practically applicable, results for such systems are probably not always comparable with the results of studies using single channels due to flow mal-distribution which are influenced by, for instance, the arrangements at inlet and outlet manifolds [22]. Inlet effects and two- and three-dimensional transport effect have also been identified to cause inconsistencies in results [23, 24].

From the literature, it appears as if little emphasis has been placed on the influence of the inlet configuration with diabatic flow in single channels. Of the studies included in Table 1, many made use of a sudden contraction inlet geometry type, but often the actual size and configuration of the inlet is not fully described. This leaves an underlying question about how the inlet geometry can affect the pressure drop and heat transfer coefficient. A need to investigate the inlet geometry was also expressed by Celata *et al.* [13].

It has been shown that on macro-scale the inlet type has a significant impact on the heat transfer, friction factor and critical Reynolds number. The influence of the inlet on transition has been investigated systematically by the laboratories of Ghajar at Oklohoma state University and Meyer at the University of Pretoria. Ghajar and co-authors [25–30] investigated the influence of different types of inlets while using a constant heat flux. Meyer and co-authors used a constant wall temperature and investigated smooth [31] and enhanced tubes [32, 33] and also investigated the use of nanofluids [34] during constant heat flux conditions. However, all this work was done on circular tube diameters larger than 5 mm. Thus, little or no work has been done on smaller diameters to investigate the influence of different types of inlets in the laminar and transitional flow regimes of rectangular type micro channels.

Table 1 Literature comparison

Year	Authors	Fluid	Channel cross-section	Inlet type	Channel material	Channels	Boundary condition	Diameter range [μm]	Relative roughness [%]	Critical Re	*f*	Nu
1981	Tuckerman and Pease [1]	Water	Rectangular	-	Fused silica	Multi	Cons. flux	86 – 95	-	2 300	-	-
1996	Peng and Peterson [2]	Water	Rectangular	SC	Stainless steel	Multi	Const. flux	133 – 267	-	2 000 – 3 000	< >	<
1999	Mala and Li [3]	Water Water	Circular Circular	SC	Fused silica Stainless steel	Single Single	Adiabatic	50 – 250 64 – 254	- -	300 – 900 500 – 1 500	> >	N/A
1999	Harms *et al.* [4]	Water	Rectangular	SC	Fused silica	Multi	Const. flux	404 – 1 923	0 - 0.02	1 500	=	≥
2000	Weilin *et al.* [5]	Water	Trapezoidal	SC	Fused silica	Single	Adiabatic	51 – 169	1.24 - 1.75	-	>	N/A
2002	Judy *et al.* [6]	Water CH_3OH C_3H_8O	Square Circular Circular	-	Fused silica Fused silica Stainless steel	Single Single Single	Adiabatic	50 – 100 15 – 150 75 – 125	- - -	2 300 2 300 2 300	= = =	N/A
2002	Hegab *et al.* [7]	R134a	Rectangular	SC	Aluminium	Multi	Const. flux	112 – 210	0.16 - 0.74	2 000 – 4 000	<	<
2004	Celata *et al.* [8]	Water	Circular	SC	Fused silica	Single	Const. temp.	80 – 166	< 0.10	1 800 – 2 500	≥	
2004	Garimella and Singhal [9]	Water	Rectangular	SC	Stainless steel	Single	Const. temp.	250 – 1 000	-	2 000	=	≥
2005	Hao *et al.* [10]	Water	Trapezoidal	-	Fused silica	Single	Adiabatic	237	0.03	1 500 – 1 800	≤	N/A
2006	Steinke and Kandlikar [11]	Water	Rectangular	SC	Fused silica	Multi	Adiabatic	26 – 222	0.20	-	<	N/A
2007	Hrnjak and Tu [12]	R134a	Rectangular	SC	Polyvinyl-chloride	Multi	Adiabatic	70 – 305	0.14 - 0.35	2 150 – 2 290	=	N/A
2009	Celata *et al.* [13]	Water	Circular	-	Nitrogen gas	Single	Adiabatic	30 - 500	0 - 1	2000 - 4500	=	N/A
2010	Natrajan and Christensen [14]	Water	Rectangular	SC	Copper	Single	Const. flux	600	0.015 - 2.51	1 800 – 1 300	=	≥
2010	Morini *et al.* [15]	Water FC-72	Circular Circular	-	Stainless steel Stainless steel	Single Single	Const. flux Const. flux	146 – 440 280	4.11 - 0.68 1.07	2 380 – 3 100 2 430	- -	>
2010	Ghajar *et al.* [16]	Water	Circular	-	Stainless steel	Single	Adiabatic	337 – 2083	1.4 - 6.5	1 300 – 4 000	> =	N/A
2011	Tam *et al.* [17]	Water	Circular	SC	Stainless steel Glass	Single	Const. temp.	750 – 2000	0.2 - 0.6	1 300 – 4 000	> =	N/A
2012	Tam *et al.* [18]	Water	Circular	SC	Stainless steel	Single	Const. flux	1000 - 2000	0.21 - 0.32	700 – 15 000	=	>=

Based on this, this study attempts to look at what the impact of the inlet geometry is on the friction factors, Nusselt numbers, and critical Reynolds number associated with a single channel for different inlet types: sudden contraction, bellmouth and swirl, for diabatic conditions.

2 Experimental apparatus and procedure

2.1 Experimental test facility

An experimental facility was designed and constructed to provide the low flow rates required to investigate the laminar and transition regimes for small hydraulic diameters. A schematic of the test facility is given in Figure 1. Water was circulated by means of an Ismatec BVP-Z standard analogue

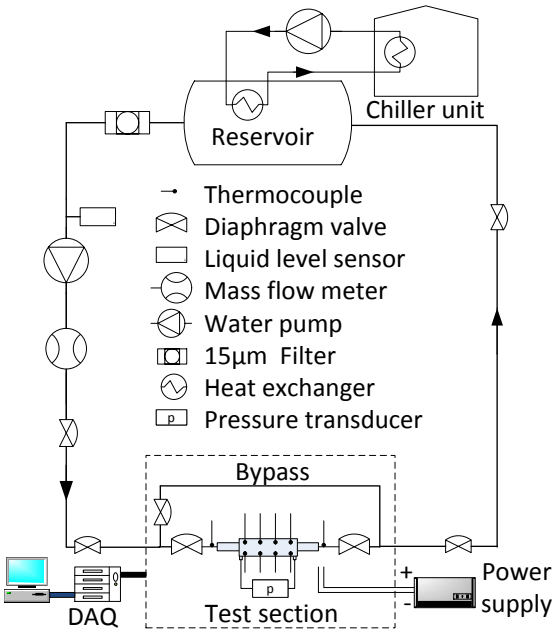

Figure 1 Experimental test facility

gear pump through the circuit. The pump had a flow rate range of 5 ml/minute to 550 ml/minute, and maximum differential pressure of 520 kPa. A coriolis mass flow meter was placed before the test section. The water was heated as it passed through the test section by means of a heater element. To maintain a stable inlet temperature to the test section, heat was removed from the water in the reservoir by means of an embedded heat exchanger. A 15 µm filter was positioned between the reservoir and the pump to trap any foreign particles. A liquid level sensor was used to detect air bubbles, which, if present could damage the pump and influence experimental data. A bypass line, which ran parallel to the test section, could be used to reroute water if necessary. The test facility was controlled and monitored using National Instruments hardware and software. The data acquisition

hardware system was interfaced to Labview software to provide controlled data logging using a graphical user interface.

2.2 Test sections

Three different rectangular channel sizes were considered with hydraulic diameters of 1.05 mm, 0.85 mm, and 0.57 mm. The detailed dimensions of the channels are given in Table 2. A separate test section was constructed for each channel diameter as is discussed below. A schematic representation of a typical test section is given in Figure 2.

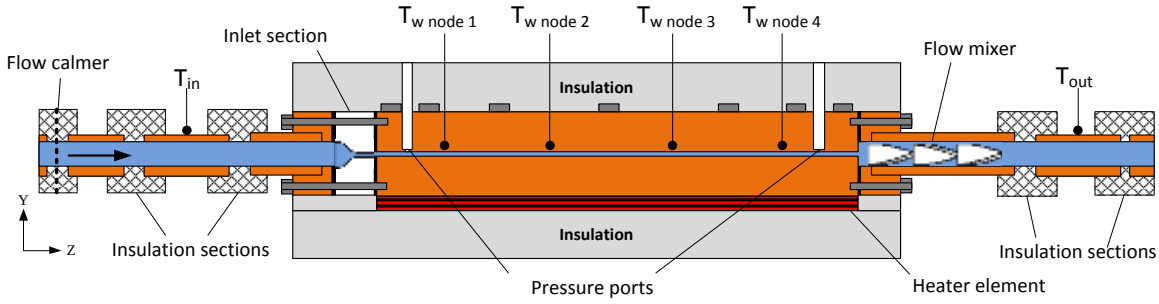

Figure 2 A typical assembled test section with a bellmouth inlet type

At the entrance to the each test section assembly, the water passed through a calming section. Thereafter, the water passed through the inlet temperature measurement section that was equipped with four T-types thermocouples (Gauge #30 of wire diameter 0.25 mm) equally spaced around the periphery of a small length of copper tube. The measurement section was thermally insulated in both the upstream and downstream directions by means of Perspex. Before entering the test channel, the water passed through an appropriate inlet section, depending on the inlet configuration under consideration. The three inlet types are discussed in more detail in sections 2.2.1 to 2.2.3.

Each channel section consisted of two copper blocks, a base block which contained the milled-out channel, and a cover (or lid) block (refer to Figure 3). The blocks were 200 mm in length (L), 20 mm in width (W_{base}) and 5 mm in height, irrespective of the channel diameter under investigation. This

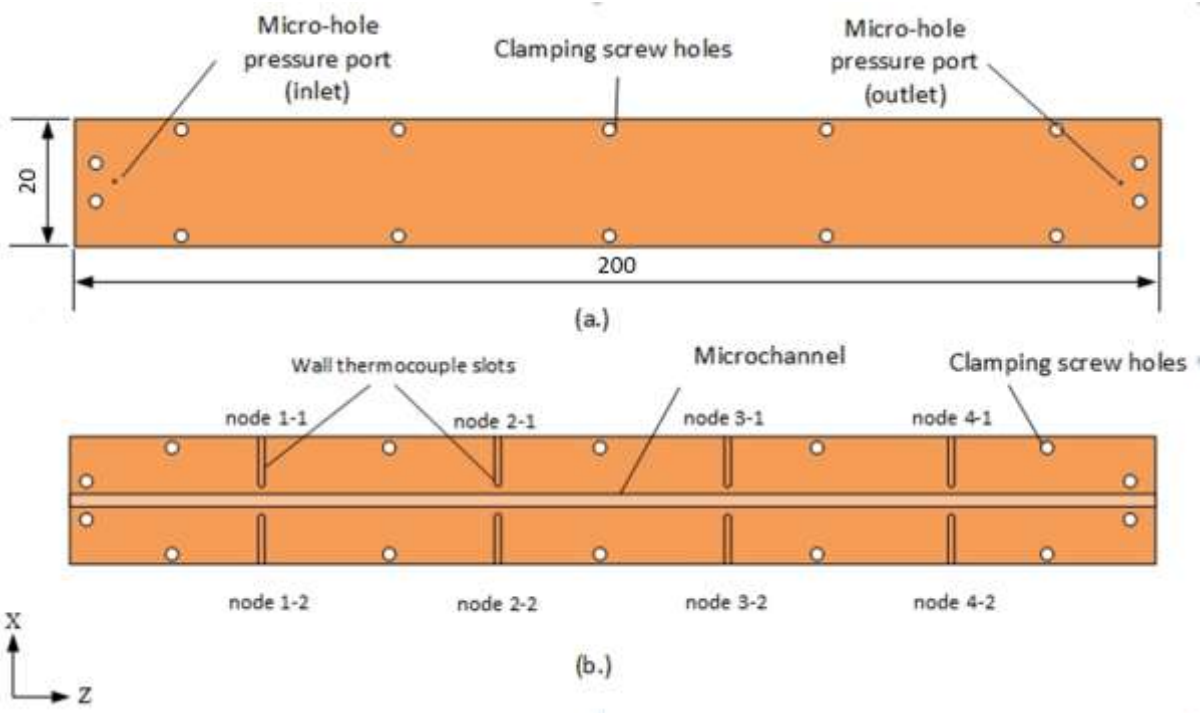

Figure 3 (a.) Test section lid block and (b.) Micro-channel base block (dimensions in mm)

resulted in length to channel diameter ratios (L/D_h) of 190, 235 and 350 for the 1.05 mm, 0.85 mm and 0.57 mm channels respectively. The surface roughness for the test sections were measured at three different locations inside each channel using a laser scanning microscope. These roughness values are also given in Table 2.

Table 2 Microchannel geometric and surface roughness description

Test section	Dimensions [mm]				Measured surface roughness [µm]				Relative roughness, $\boldsymbol{\varepsilon}$, [-]
	Width,	Height,	PTFE layer	D_h*	Inlet	Middle	Outlet	Average	
1	1.044	1.001	0.05	1.05	2.527	2.172	2.267	2.322	0.00221
2	0.833	0.810		0.85	2.625	3.177	2.071	2.624	0.00309
3	0.522	0.568		0.57	4.719	3.885	3.933	4.179	0.00733
*D_h is calculated with the total channel height including the thickness of the PTFE layer									

Each base block contained a set of four milled slots (0.8 mm wide) on either side of the channel to accommodate embedded T-type thermocouples (refer to the node numbers in Figure 3). The vertical

depths of the slots were different for each channel diameter to ensure that the thermocouple tips would be located in the midpoint of the channel wall height. These thermocouples (Gauge #40), each having a diameter of 0.08 mm, were used to measure the side wall temperatures of each channel. The slots were milled to distance of 0.25 mm away from the channel wall. Care was taken during thermocouple installation to ensure the correct positioning of the thermocouple tips. Once the thermocouple tips were positioned, a quick-drying adhesive with a thermal conductivity of approximately 0.5 W/mK was applied, and any excess adhesive was removed after curing. The final distance of the thermocouple tips from the channel inner wall was measured to be 0.4 mm. Since the accuracy of the wall temperature measurement is vital to the determination of the Nusselt number, copper was selected for its high thermal conductivity for the base material in which the channel was machined into.

A sensitivity analysis was done using a computational fluid dynamics model to determine the wall temperature profile for different heat fluxes at increments of less than 0.15 mm for the approximate convective heat transfer coefficients obtained in this study. This indicated that at the position of the thermocouple tip the temperature would be lower than at the wetted wall by less than 0.02 °C. This value was much lower than the thermocouple uncertainty and was therefore negated from the results analysis. The temperature distribution around the circumference of the tube was also checked numerically and found to be in the order of 0.1°C on the outer circumference of the copper blocks (base block and lid block). This was also validated by direct thermocouple measurement which gave temperature variations of less than 0.2°C. Based on this it was assumed that the temperature variation around the circumference of the wetted channel surface was negligible and that the temperatures taken on the side walls were representative of the local circumferential wall temperature.

The lid block (which was re-used for all test sections) sealed the test section from above. The lid contained two holes of diameter 0.1 mm, each located 5 mm from the lid ends. Once the lid was secured to the base block, these holes lined up to the centre of the channel and allowed the differential pressure to be measured directly from the channel. For this purpose, a Validyne DP15 differential pressure transducer was used. To ensure that accurate pressure measurements were made, adiabatic

tests were run on the different micro-channels for the sudden contraction inlet configurations. The initial diaphragm was chosen based on the theoretical pressure drop calculations using macro-channel theory as a first approximation. Once a few points were measured and logged over the desired range of the experiments, the data was analysed and the final diaphragms were chosen that could accurately measure friction factors in both the laminar and transition regimes. Two diaphragms were used – a gauge #34 for low pressure drop measurements up to 22 kPa and a gauge #44 for high pressure drop measurements up to 220 kPa. The 22 kPa diaphragm was used for the 1.05 mm test section, while the 220 kPa was used for the 0.85 mm and 0.57 mm test sections. Uncertainty analyses were conducted on measured values and are discussed in more detail in section 3.3.

Polytetrafluoroethylene (PTFE) tape (having a thickness of 0.05 mm) was used as a gasket between the base block and the lid block and was taken into consideration with the dimensions in Table 2. Care was taken to ensure that the tape did not encroach on the micro-channel area, ensuring that all four sides of the channel were exposed to the copper. The lid was fastened to the base block in sequence by means of bolts to ensure an even distribution of force.

A flow mixer was placed directly after the channel section, to mix the water exiting the test section to allow for more accurate bulk exit temperature measurements by disturbing the boundary layer. The water exit temperature was measured in the same fashion as the inlet temperature.

An adjustable 800 W direct current power supply was used to provide constant power to the heater element. The heater element was manufactured from constantan wire, and positioned below the test section. The constantan wire was insulated with a thin layer of Teflon, preventing any electric current from passing through to the test section. The heating element was designed to deliver a uniform surface heat flux to the bottom surface of the base block. The test section was thermally insulated in all directions using high density polystyrene. The heat loss to the surroundings was monitored by measuring the temperature difference across the insulation layer.

Inlet sections were manufactured according to the dimension of the channel and are discussed shortly. They were interchangeable and were attached to the copper channel section by means of stainless

steel screws. PTFE tape and a Viton washer were used as gasket material. The screws used to mount the inlet section to the test channels resulted in a heat loss of less than 1% of the produced heat in the heating element towards the inlet sections.

2.2.1 Sudden contraction inlet

The sudden contraction inlet reduced the flow passage diameter from the circular system piping diameter of 6.35 mm to the channel diameter (rectangular), as shown in Figure 4a. Each test section had its own inlet. The inlet was constructed from copper. The lengths of the inlets were 10 mm for all three test sections. The sudden contraction sections had a dual function. Apart from being an inlet geometry, it was also used as the system interface component for the bellmouth inlet, as is shown in Figure 2 and Figure 4b.

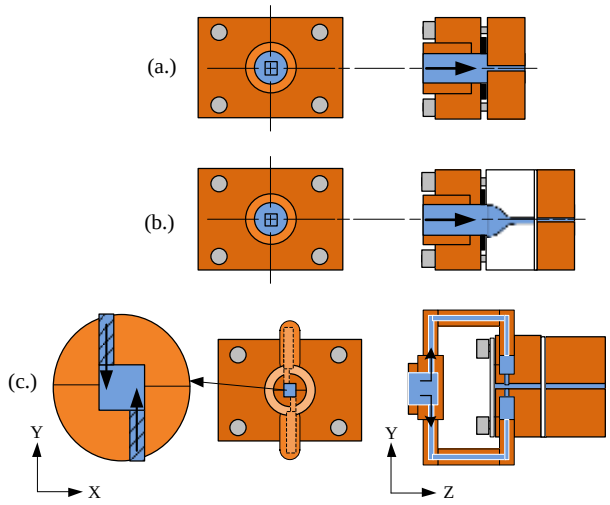

Figure 4 Geometries of the (a.) sudden contraction inlet type, (b.) bellmouth inlet type and (c.) swirl inlet type

2.2.2 Bellmouth inlet

The bellmouth inlet sections were designed to contour the water from the system piping to the micro-channel along a designed profile, as shown in Figure 4b. The inlet profiles were designed using the method prescribed by Morel [35]. This resulted in different diameter and area contraction ratios for each test section as are given in Table 3. The same design methods were also used by Tam and Ghajar [28] and Olivier and Meyer [31] on macro-channel experimentation.

Table 3 Bellmouth contraction ratios

D_h $[mm]$	Diameter Contraction Ratio	Area Contraction Ratio
1.05	5	33
0.85	6.25	50
0.57	10	111

For manufacturing purposes, the inlets were made in two halves, a bottom half and a top half. These sections were manufactured from Perspex by using a CNC machine. The Perspex reduced the heat transfer through the inlet section and allowed the two halves to be glued using adhesive. Each half was 15 mm in length to accommodate the profile shape. A rig and rectangular alignment tools were made to align the two halves to each other as well as to the channel. The alignment tool was manufactured 30 μm smaller than the micro-channel width and height, providing a maximum misalignment of 30 μm. This translated into a maximum of 3% and 5 % misalignment for the largest and smallest diameter cases respectively.

2.2.3 Swirl inlet

The swirl inlet was investigated for the 1.05 mm test section only, due to manufacturing and pressure drop constraints. This inlet section was made from copper to withstand the higher operating pressure which was required to sustain flow through the test section with this inlet type. It was intended to increase the heat transfer coefficient by causing the fluid to spiral as it flowed through the micro-channel. Two off-centre in-plane holes were used to create the spiral flow (see Figure 4c). The holes were located at the bottom and top walls on the opposite edges of the inlet channel at one end of the inlet. The centres of the holes were located 0.25 mm away from their respective channel side walls. Water entered from each hole and travelled around the periphery of the micro-channel wall, resulting in a swirl flow pattern.

The design of the swirl inlet was based on the work of Aydin and Baki [36], who used a similar design for counter flow vortex tubes to compare the effect of different inlet angles on swirl flow. The design used in this study was checked for swirl intensity by using a computational fluid dynamics

model before it was manufactured. Numerical results indicated that significant swirl is present, but that it dissipates along the length of the channel. The inlet was aligned to the test section by using the same method as with the bellmouth inlet type.

2.3 Experimental procedure

Experimental test sets consisted of approximately 25 data points, each at a different water mass flow rate. Each data point was obtained by averaging 100 steady state measurements taken over a timespan of ten seconds at a frequency of 10 Hz. A Reynolds number increment of approximately 80 to 120 was used, starting at a Reynolds number of approximately 2 800 and ending at a Reynolds number of above 300. Experiments were mostly conducted from a high Reynolds number to a low Reynolds number to limit the heat storage effects of the channel thermal insulation. The effects of hysteresis were not specifically investigated in this study but repeatability was checked whereby the test section was dissembled and reassembled before tests were repeated.

The energy balance was calculated with equation 1.

$$eb = \frac{\bar{\dot{Q}}_{heater} - \bar{\dot{Q}}_{water}}{\bar{\dot{Q}}_{heater}} \tag{1}$$

This gives a measure of the proportion of the input heat rate, $\bar{\dot{Q}}_{heater}$, lost to, or gained from the surroundings. Measured values were displayed on the computer screen, along with graphs which plotted the history over the previous 1000 measurements. When the variation of the energy balance was consistent for approximately 2 minutes, the mass flow rate was constant, the variations of the bulk inlet and outlet temperatures were within ±0.04 °C, the wall temperatures, insulation temperatures, mass flow rate, and pressure drop data were logged.

3. Data reduction and uncertainty analysis

3.1 Nusselt numbers

The heat input used to determine the energy balance was equal to the power supply output and was calculated using equation 2.

$$\bar{\dot{Q}}_{heater} = \bar{V}\bar{I} \tag{2}$$

The base surface heat flux of the base block was calculated using equation 3. This was based on the power transferred through contact area between the heater element and the base of the micro-channel block.

$$\bar{\dot{Q}}''_{base} = \frac{\bar{\dot{Q}}_{heater}}{W_{base}L} \tag{3}$$

The other heat flux value of interest was the wetted surface channel heat flux based on the channel wall area, calculated using equation 4. The three wetted surface heat fluxes considered where kept approximately constant for the different micro-channel experiments, as shown in Table 4.

Table 4 Experimental equipment and dimensional uncertainties

D_h [mm]		Channel surface heat flux cases		
	Approximate $\bar{\dot{Q}}''_{wetted}$ [kW/m^2]:	**24**	**36**	**48**
1.05	$\bar{\dot{Q}}_{heater}$ [W]	20	30	40
	$\bar{\dot{Q}}''_{base}$ [kW/m^2]	5	7.5	10
0.85 mm	$\bar{\dot{Q}}_{heater}$ [W]	16	24	32
	$\bar{\dot{Q}}''_{base}$ [kW/m^2]	4	6	8
0.57	$\bar{\dot{Q}}_{heater}$[W]	10	15	20
	$\bar{\dot{Q}}''_{base}$ [kW/m^2]	2.5	3.75	5

$$\bar{\dot{Q}}''_{wetted} = \frac{\bar{\dot{Q}}_{heater}}{P_{channel}L} \tag{4}$$

The heat transferred to the fluid was calculated with equation 5. Inlet and outlet temperatures were determined by averaging the measurements obtained with the respective four thermocouples at the inlet and outlet measuring point. The mass flow rate was from the measurements of the Coriolis flow meter. The specific heat properties of water were calculated at the effective bulk fluid temperature using the equations derived by Popiel and Wojtkowiak [37].

$$\bar{\dot{Q}}_{water} = \dot{m}C_p(\bar{T}_{out} - \bar{T}_{in}) \tag{5}$$

The average wall temperature was found to be non-linear and was calculated using the trapezoidal rule, providing a more accurate average wall temperature measurement. This is given in equation 6. Due to the layout of the wall thermocouples, the average nodal temperature values ($\bar{T}_{w\ node_n}$) at the entrance and exit of the test section (n = 0 and n = 5 respectively) were extrapolated from the adjacent measurement points. This was done by linearly extrapolating T_{node1} and T_{node2} to determine T_{node0} (entrance wall temperature) and extrapolating T_{node3} and T_{node4} to determine T_{node5} (exit wall temperature). The extrapolation method was employed based on the thermal profile of the average wall temperatures at each measuring location. This was monitored for each experiment, and a similar trend in the profiles led the decision to split the linear extrapolation between the first two and the last two thermocouples.

$$\bar{T}_w = \frac{1}{n}\left(\frac{1}{2}\bar{T}_{w\ node_0} + \bar{T}_{w\ node_1} + \bar{T}_{w\ node_2} + \cdots + \bar{T}_{w\ node_{n-1}} + \frac{1}{2}\bar{T}_{w\ node_n}\right) \tag{6}$$

The heat transfer $\bar{\dot{Q}}_{water}$ was also used to calculate the average heat transfer coefficient of the micro-channel using equation 7. The average surface area (A_s) was based on the channel inner wall surface area.

$$\bar{h} = \frac{\bar{\dot{Q}}_{water}}{A_s(\bar{T}_w - \bar{T}_b)} \tag{7}$$

The representative average bulk fluid temperature is dependent on the bulk temperature profile along the length of the channel and is affected by the presence of axial wall conduction. Since a copper base material was used, care was taken in this regard because experimental heat transfer results in micro-channels have been shown to be influenced by the effect of axial heat conduction. The axial heat conduction severity can be determined using equation 8 to determine the ratio between the conductive heat transferred in the surrounding material and the convective heat transferred in the fluid. If the ratio, *M*, exceeds 0.01 (or 1%), the wall conduction may play an important role when analysing the experimental data.

$$M = \left(\frac{k_s}{k_f}\right)\left(\frac{D_o^2 - D_i^2}{D_i L}\right)\frac{1}{Re\ Pr} \tag{8}$$

In this study the influence of the axial wall conduction was addressed by determining the bulk fluid temperature profile using a hybrid-numerical data-processing method based on the method of Maranzana *et al*. [21]. In this study a uniform heat transfer coefficient was adopted as this was shown to only have a very small influence on the calculated temperature field [21]. The experimentally measured $\bar{T}_{in}$, $\bar{T}_{out}$, $\dot{m}$, and $\bar{T}_w$ values were used as input constraints and the local bulk fluid temperature was calculated along the length of the channel. Since this is a well constraint problem, the effective average bulk fluid temperature could be determined. Figure 5 shows the result of two

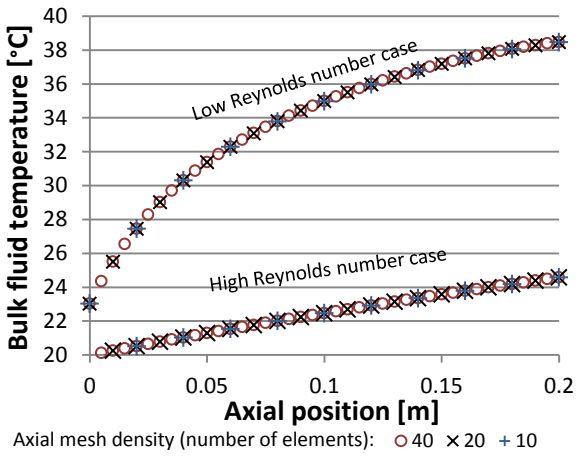

Figure 5 Mesh-dependence of numerically based bulk fluid temperature profile for two arbitrary Reynolds number cases

example cases (each at a set of different axial numerical mesh densities), one with a relatively low Reynolds number resulting in significant axial heat conduction, and another with a relatively high Reynolds number where axial heat conduction was not significant. For the low Reynolds number example case the effective bulk fluid temperature was 33.82°C, while the arithmetic average of the inlet and the outlet temperatures would have resulted in a value of 30.74°C which would have had a significant impact on the calculated heat transfer coefficient. For the high Reynolds number case the arithmetic average would have resulted in a much smaller error since the bulk fluid temperature is almost exactly linear. Irrespective of the Reynolds number or the value of *M*, all experimental cases were analysed using the same hybrid numerical approach. In the transitional flow regime, of importance to this paper, the effective heat transfer coefficient was altered by between 0.4% and 5% by this procedure but did not alter the critical Reynolds number by more than 0.3%.

The average Nusselt number, given by equation 9, was determined by using the calculated heat transfer coefficient, based on the hydraulic diameter, D_h, of the channel.

$$\overline{Nu} = \frac{\bar{h} D_h}{k_f} \tag{9}$$

The thermal conductivity of the water was obtained at the effective average bulk temperature from the equations proposed by Popiel and Wojtkowiak [37]. The obtained Nusselt numbers were compared with the developing flow equation with uniform heat flux for simultaneous thermal and hydrodynamic development given in equation 10, while the turbulent results were compared with the Gnielinski equation [38] given in equation 11.

$$\overline{Nu}_{lam} = 4.36 + \frac{0.036\left(\frac{D_h}{L}\right) Re_{D_h} Pr}{1 + 0.0011\left(\frac{D_L}{L}\right) Re_{D_h} Pr} \tag{10}$$

$$\overline{Nu}_{Gn} = \frac{(f/8)\left(Re_{D_h} - 1\,000\right)Pr}{1 + 12.7\left(\sqrt{f/8}\right)^{\frac{1}{2}}\left(Pr^{\frac{2}{3}} - 1\right)} \tag{11}$$

3.2 Friction factors

The Darcy-Weisbach friction factor was used in this study and determined from the measured data by using equation 12. The pressure drop was obtained from the measured pressure drop between the inlet and the outlet of the channel. The average velocity was determined from the measured mass flow rate and the cross sectional area of the channel. All material properties were evaluated at the effective average bulk fluid temperature.

$$f = \Delta P \frac{D_h}{L_p} \frac{2}{\rho v^2} \tag{12}$$

Even though this investigation was mainly focused on the diabatic transitional flow regime behaviour, selected adiabatic cases were considered to determine the accuracy of the system and to ensure the correct pressure diaphragms were used for each micro-channel.

Obtained laminar friction factors were compared to the Shah and London [39] relationship for adiabatic rectangular channels, given by equation 13.

$$f_{SL} = 96/Re_{D_h}(1 - 1.3553\alpha + 1.946\alpha^2 - 1.7012\alpha^3 + 0.9564\alpha^4 - 0.2537\alpha^5) \tag{13}$$

Here α is the channel aspect ratio defined as the minor dimension over the major dimension. Since the the L/D_h ratios considered in this study were not large enough to constitute fully developed flow, the laminar adiabatic friction factors were also compared to the model proposed by Muzychka and Yovanovich [40] for developing flow in non-circular ducts given in equation 14.

$$f_{MY} = \frac{1}{Re_{D_h}} \left[\left(\frac{3.44}{L^+} \right)^2 + \left(\frac{12}{\sqrt{\alpha}(1+\alpha)\left[1 - \frac{192\alpha}{\pi^5} tanh\left(\frac{\pi}{2\alpha}\right)\right]} \right)^2 \right]^{\frac{1}{2}} \tag{14}$$

With L^+ being the non-dimensional length defined as:

$$L^+ = \frac{L/D_h}{Re} \tag{15}$$

Transition and turbulent results were compared to the Blasius equation given by equation 16.

$$f_{Bl} = 0.3164/Re_{D_h}{}^{0.25} \quad (16)$$

Since the friction factors calculated with equations 13 and 14 are based on material properties evaluated at the bulk fluid temperature, friction factor calculated from diabatic data will be different from adiabatic friction factors. This is because the fluid properties at the wall will be different from those at the bulk fluid temperature. A method with which the diabatic obtained results can be adjusted in terms of the viscosity ratio in terms of the bulk fluid temperature versus the wall temperature is presented by Kakaç *et al.*[41] and as shown in equation (17).

$$f = f_{diabatic}\left(\frac{\mu_b}{\mu_w}\right)^m \quad (17)$$

Exponent m differs for different flow conditions and channel configurations. For instance, for fully developed laminar flow in a circular tube a value of m = -0.58 was proposed by Deissler (1958) as reported by Kakaç *et al.*[41]. In this study, the three heat flux levels that were considered produced sufficient variation in the viscosity ratio to determine approximate ranges for m. This will be elaborated on briefly in section 4.1 along with the main body of results.

Table 5 Result uncertainty ranges and average uncertainty for the different test sections

	Uncertainty	Operating range	Uncertainty range
Thermocouples	0.1°C	20°C – 57 °C	0.18% – 0.50%
Pressure transducer (gauge #34)	57.6 Pa	700 Pa – 20 000 Pa	0.29% – 8.23%
Pressure transducer (gauge #44)	435.6 Pa	1000 Pa – 160 000 Pa	0.27% – 43.6%
Mass flow meter	0.000027 kg/s	0.00013 kg/s – 0.0027 kg/s	0.1% – 52%
Hydraulic diameter	0.01 mm	-	0.95% – 1.75%
Length	0.2 mm	-	0.10%

3.3 Uncertainty Analysis

The method presented by Moffat [42] was used to determine the uncertainty of the calculated results. Table 5 gives the experimental equipment and dimensional uncertainties while Table 6 gives the calculated value uncertainties. Due to the higher measurement uncertainties at low mass flow rates

and low pressure differences, the Friction factor and Nusselt number uncertainties were the highest at low Reynolds numbers. However, in the transitional region, uncertainties for the Nusselt number and, friction factor were concentrated around the lower uncertainty values given in Table 6.

Table 6 Heat flux inputs to the test sections

Hydraulic diameter	Result	Result range [-]	Uncertainty range [±]	Average uncertainty [±]
1.05 mm	*Re*	365 – 2 620	2.3% – 26%	6.1%
	f	0.028 – 0.14	2.2% – 27%	4.2%
	Nu	4 – 22	5.0% – 26%	7.6%
	j	0.0018 – 0.008	5.7% – 37%	9.0%
0.85 mm	*Re*	371 – 3 000	2.5% – 30%	7.1%
	f	0.029 – 0.094	2.8% – 51%	10%
	Nu	4.4 – 22	6.5% – 31%	13%
	j	0.0017 – 0.008	7.1% – 43%	15%
0.57 mm	*Re*	357 – 2 833	3.0% – 45%	12%
	f	0.038 – 0.13	4.0% – 46%	12%
	Nu	4.8 – 22	13% – 47%	19%
	j	0.0021 – 0.008	15% – 64%	23%

4. Results and discussion

4.1 Diabatic versus adiabatic friction factors.

Adiabatic as well as diabatic test were conducted on some of the test section in order to ascertain whether the presence of heat transfer affect the onset of transition and to what extent the measured friction factor is affected. Adiabatic test were also used to validate the test facility. For the sudden contraction inlet type, full sets of adiabatic experiments were conducted on the 1.05 mm and 0.57 mm channels while for the bellmouth inlet this was done for the 1.05 mm channel. For the 0.85 mm

channel and the swirl inlet only discrete Reynolds numbers were chosen to verify correct operation and pressure ranges.

Diabatic experiments were conducted at different heat rates applied to the lower surface of the base copper block as is described in Table 4. As per equation 17 it was found that the measured diabatic friction factors differed from the adiabatic friction factors for the same channel and inlet section combination. Directly obtained friction factors decreased in value as the heat flux level was increased. For the heat fluxes considered in this study a decrease in the friction factor of up to 15% in terms of the adiabatic friction factor was noticed at any given Reynolds number. It was found that the value of m in equation 17 (that resulted in the adjusted diabatic friction factors agreeing with the adiabatic friction factors) were dependent on the mass flow rate. For Reynolds numbers increasing from 500 to 1 500, it was found for the 1.05 mm channel with the sudden contraction inlet that the value of m increased in a narrow band between 0.55 and 0.65. For the same channel with a Bellmouth inlet, m increased in a much wider band from 0.25 to 0.65. For the 0.57 mm channel with a sudden contraction inlet m decreased in an even wider band from 1 to 0.4. For Reynolds numbers above 2000 different values of m were obtained depending on the channel diameter and the inlet.

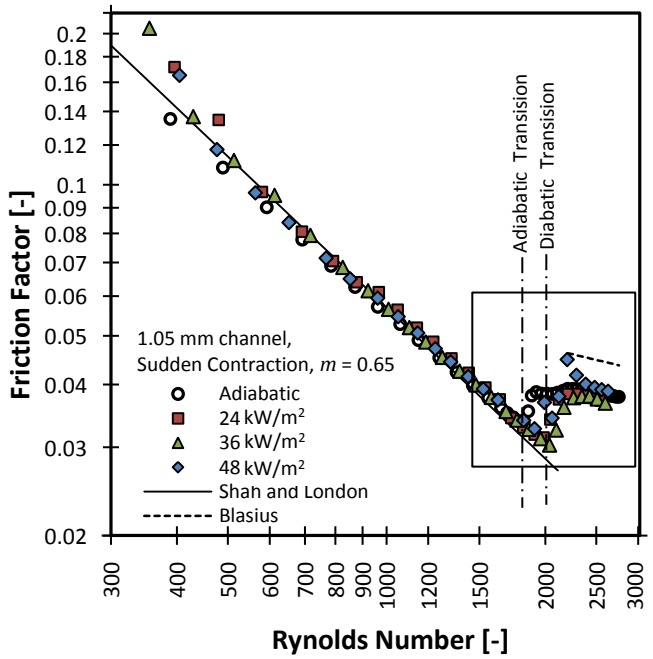

Figure 6 Adiabatic and diabatic friction factor results for the 1.05 mm test section with a sudden contraction inlet with m = 0.65

A comparison of the adiabatic and diabatic friction factors with m = 0.65 are presented in Figure 6 for the sudden contraction inlet with the 1.05 mm channel, with Figure 7 showing an enlargement of the transitional flow regime region. Uncertainty bars are omitted from these figures for clarity reasons, but are included in subsequent plots. In Figure 6 it is seen that the laminar adiabatic friction factors agreed well with the Shah and London correlation prediction (within 8%) and that transition commenced at a Reynolds number of 1 800. At a Reynolds number of about 2 500 transition appears to be complete and the adiabatic friction factor gradient was similar to that of the Blasius correlation predictions, however, they were over-predicted by about 25% by the Blasius equation. For the diabatic friction factors, it can be seen that the transition onset was postposed to a Reynolds number of 2 000. This was found to be about constant to all three heat flux conditions considered as are discussed in more detail in section 4.3.1. In Figure 7 containing a zoomed in portion the adiabatic

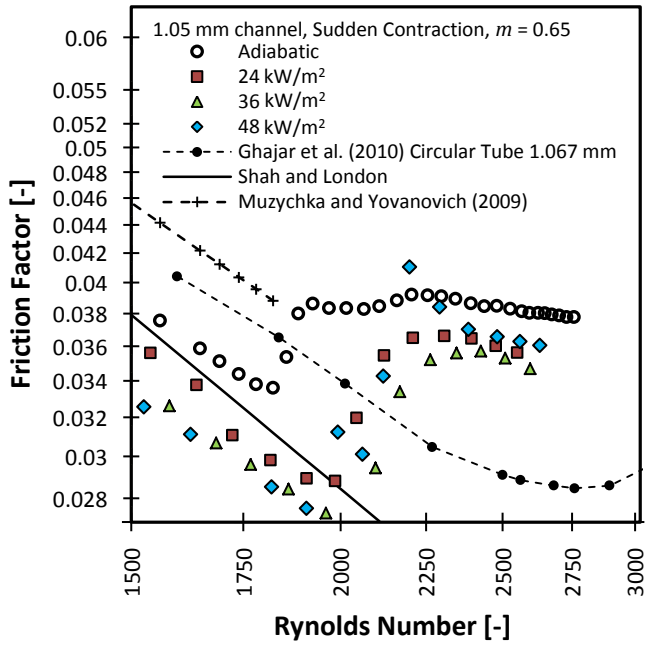

Figure 7 Zoomed in region for comparison of adiabatic and diabatic friction factors for the 1.05 mm test section with a sudden contraction inlet with m = 0.65

friction factors can be compared more closely with the friction factor measurements taken by Ghajar *et al.* [16] on fully developed flow of water in a circular tube with a diameter of 1.067 mm, similar to the hydraulic diameter of our channel. Also in this figure are the predictions of a model by Muzychka and Yovanovich [40] for developing flow in a square channel. The adiabatic friction factors lie

between the predictions of the Shah and London and the Muzychka and Yovanovich models. It can also be seen that the transition observed in the rectangular channel were earlier and was more distinct than the smoother transition observed by Ghajar *et al*.[16] (measured with a 34.5 kPa diaphragm differential pressure transducer). Based on the relative good agreement between the experimental measurements and previous results and existing models, it indicates that the experimental facility and method was suitable to investigate the transitional flow regime.

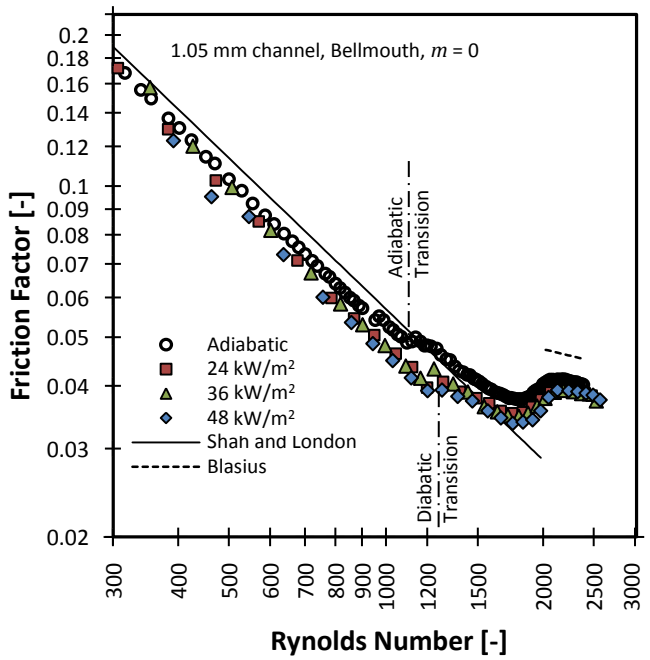

Figure 8 Adiabatic and diabatic friction factor results for the 1.05 mm test section with a bellmouth inlet with $m = 0$

Figure 8 presents the adiabatic and diabatic obtained friction factors for the 1.05 mm channel for the Bellmouth inlet type. In this figure $m = 0$, which explains why the diabatic friction factors are lower than the adiabatic friction factors. It can be seen that the adiabatic friction factor data demonstrates a disturbance at a Reynolds number of about 1 100, which could be the onset of transition. A more-obvious change in behaviour is noticeable at a Reynolds number of about 1 650. When considering the diabatic data, a similar type profile is observed, but delayed. The first disturbance in the trend is now visible at a Reynolds number of 1 250 with the second behavioural change occurring at a Reynolds number of about 1 650. The adiabatic friction factors for flow rates above a Reynolds number of 2000 were over-predicted by the Blasius equation by approximately 10%.

By comparing the data given in Figures 6 and 8 it was found that the diabatic condition transitions occurred at higher Reynolds numbers compared to the adiabatic conditions, and that the initial onset of transition with the Bellmouth inlet type occurred earlier than the transition with the sudden contraction. Since the value of m needed to match the diabatic friction factors with the adiabatic friction factors are not consistent for all flow rates (especially in the transitional flow regime), channel diameters and inlet types, the rest of the friction factor data presented in this paper will be for $m = 0$. A separate and more in-depth investigation in the influence of the fluid properties are needed to determine how the diabatic and adiabatic friction factors should be related to each other. Also, since this investigation is more interested in the influence of the inlet geometry on the onset of turbulence, it is deemed suitable to ignore the wall temperature influence on the friction factor for now.

4.2 Sudden contraction inlet results

Diabatic friction factor and the Nusselt number results for the sudden contraction inlet type are presented in Figure 9 and Figure 10 respectively for all three diameters with a wetted channel wall

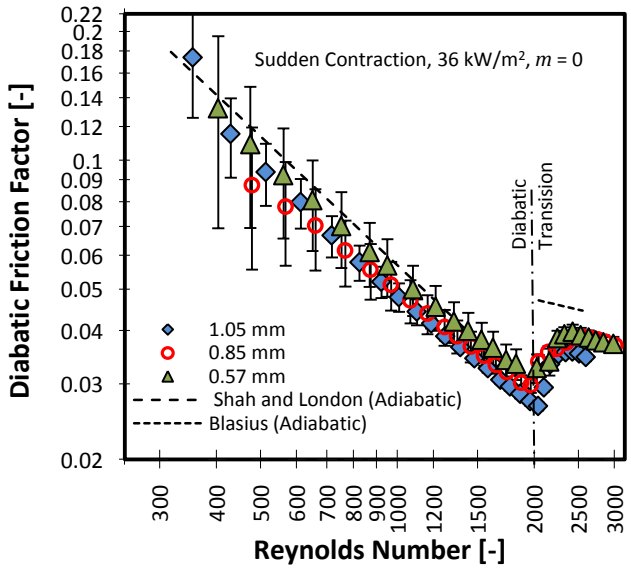

Figure 9 Diabatic friction factors for different diameters with a sudden contraction inlet section at a wetted surface heat flux of 36 kW/m^2

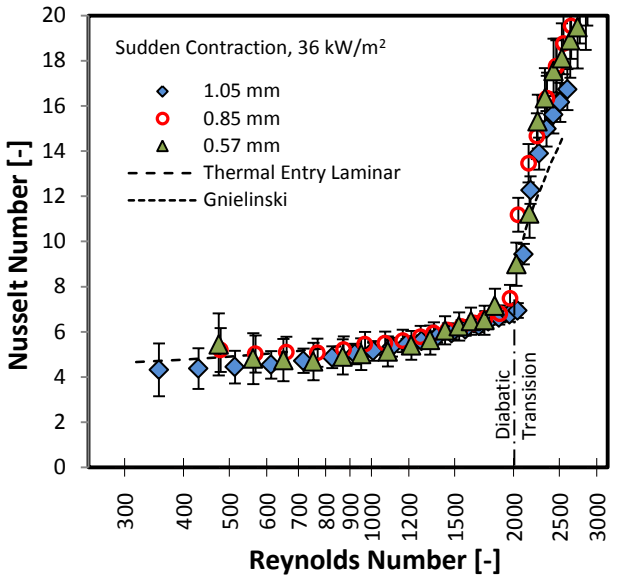

Figure 10 Nusselt numbers for different diameters with a sudden contraction inlet section at a wetted surface heat flux of 36 kW/m^2

heat flux of 36 kW/m^2. The Shah and London predictions for the 1.05 mm channel and the Blasius equation are once again included with the friction factor for comparative purposes. No conclusion could be drawn as to the dependence of the friction factor on the channel hydraulic diameter because of the diabatic fluid behaviour as discussed earlier. The friction factor results at different channel diameters were found to be within 10% of each other for all regimes. Friction factor deviation between different diameter cases was higher for Reynolds numbers below 500. This was attributed to the low stability of the pressure measurements at low flow rates and the higher uncertainties (Table 5) at low Reynolds numbers. The transition regime began between Reynolds numbers of 1 950 and 2 000 for all diameters. This agrees well with the literature of Céngel [43] and Olivier and Meyer [31] and Meyer and Olivier [32, 33] for macro-channel flow. The transition regime lasted for a very short Reynolds number range, and it appears as if transition was complete at a Reynolds number of 2 300 for all test sections. Measured diabatic friction factors in the laminar regime were over predicted by the Shah and London correlation by up to 15% for all channels, with an average error of 11%.

Considering Figure 10, Nusselt numbers in the laminar regime were affected by the thermal and hydrodynamic entrance lengths, resulting in the Nusselt number exhibiting an increasing trend. For comparison purposes the thermal entry Nusselt numbers from equation 10 are also included. It can be

seen that there was relatively good agreement between the experimental measurements and the predictions of equation 10 with 95% of laminar values agreeing within 10%. Nusselt numbers for the different diameters deviated by up to 10% from each other at Reynolds numbers below 1950.

The Nusselt number transition commenced at the same Reynolds number as was the case with the friction factors: between 1 950 and 2 000. As with the friction factor behaviour, the transition based on the Nusselt number was very abrupt. It was found that the Nusselt numbers for Reynolds numbers above 2 000 were under-predicted by the Gnielinski equation for all diameters by between 12% and 25%.

4.2.2 Bellmouth inlet results

The bellmouth inlet section type was investigated for all three channel diameters. Diabatic friction factor and Nusselt number results are given in Figure 11 and Figure12 respectively for a wetted surface heat flux of 36 kW/m^2. Similar as with the sudden contraction inlet, diabatic friction factors in the laminar regime were over-predicted by the adiabatic Shah and London correlation due to the wall temperature dependence.

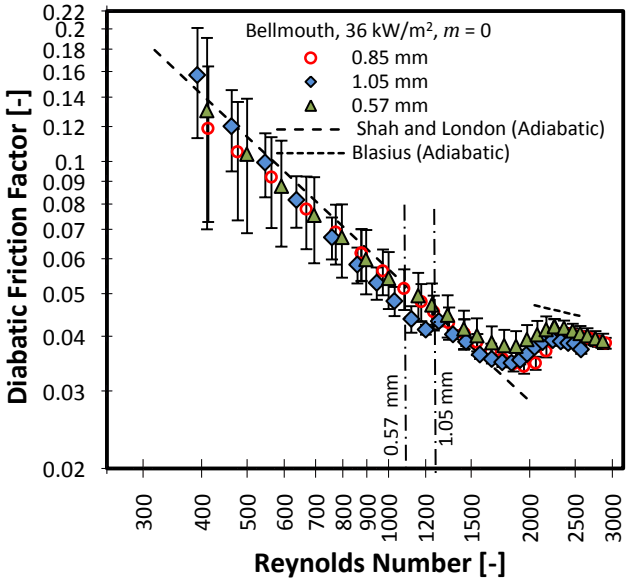

Figure 11 Diabatic friction factors for different diameters with a bellmouth inlet section at a wetted surface heat flux of 36 kW/m^2

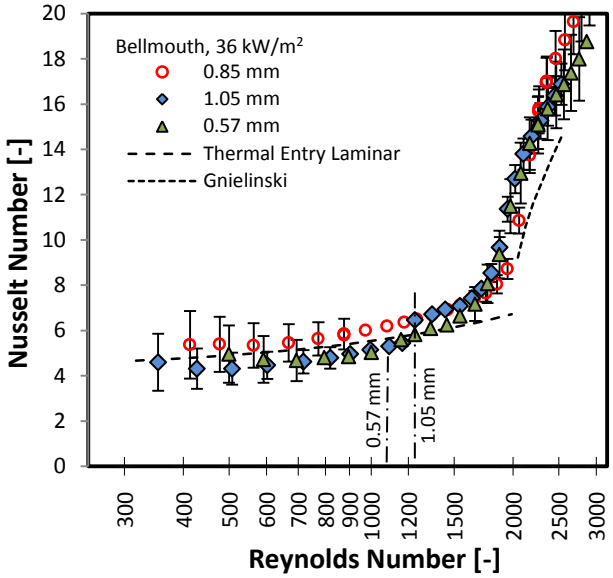

Figure 12 Nusselt numbers for different diameters inlet section at a wetted surface heat flux of 36 kW/m^2

As was mentioned earlier with reference to Figure 8, the Bellmouth inlet type exhibited a different type of transition regime result profile than what was observed with the sudden contraction inlet type. Bellmouth results indicated that the transition regime commenced at a Reynolds number of between 1 100 and 1 280 depending on the channel diameter as are indicated in Figures 11 and 12. The transition was complete at roughly Re = 2 300, similar as with the sudden contraction inlet. However, the transition with the bellmouth inlet geometry spanned a larger Reynolds number range: commencing at a lower Reynolds number while having a smooth transition to turbulence compared with the sudden contraction inlet where the transition regime was very abrupt. For Reynolds numbers above 2 300 friction factors were again over-predicted by the Blasius equation by up to 25%.

Laminar flow regime Nusselt numbers were found to be similar in magnitude to those of the sudden contraction inlet. The Nusselt numbers were also found to be independent of the heat flux input. Early onset of the transition was also exhibited in the Nusselt number results and was found to occur at the same Reynolds numbers as were the case with the friction factor results. This indicates a definite modification in the flow behaviour since it was observed on both the pressure drop measurements as well as the wall temperature readings. Nusselt number transition also stabilized at approximately Re = 2 300, similar to the sudden contraction inlet. Nusselt numbers for Reynolds numbers above 2 300

were under-predicted by the Gnielinski equation. Results for the different diameters were consistent in terms of magnitude with each other.

The results of this study are different than those of the work done by Meyer and co-authors [31–33] and Ghajar and co-authors [25–30]. In these studies for larger scaled channels the bellmouth inlet type delayed the onset of transition and in contrary, the laminar regime was shortened by the presence of the bellmouth inlet type. Possible reasons might be that that the preceding studies used circular tubes where-as rectangular channels were used here. There might also be a geometric size relationship between the critical Reynolds number and for instance the channel diameter. This is based on the observation that the 0.57 mm channel transition occurred earlier than for the 1.05 mm channel which had a different contraction ratio as are given in Table 3.

4.2.3 Swirl inlet results

As mentioned earlier, the swirl inlet type was only investigated with the 1.05 mm channel. Friction factor and Nusselt number results are given in Figure 13 and Figure 14 respectively for all three wetted surface heat flux levels. It was found that the in-channel pressure drop was higher with the swirl inlet than was the case with the sudden contraction and bellmouth inlet sections. Due to this,

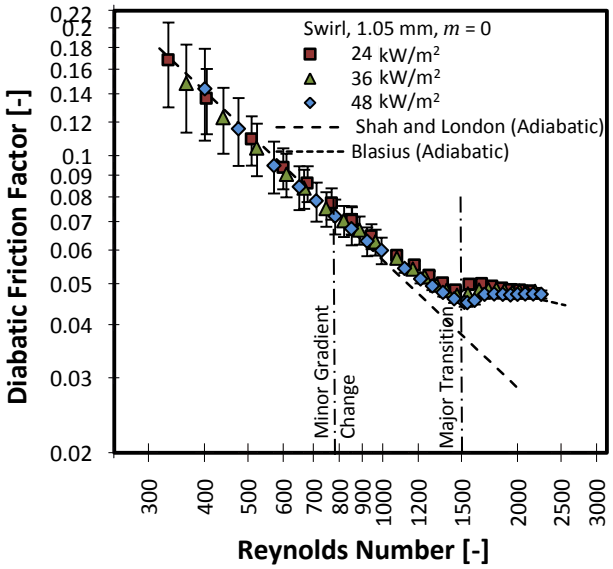

Figure 13 Diabatic friction factors with a swirl inlet section for the 1.05 mm test section at different wetted surface heat fluxes

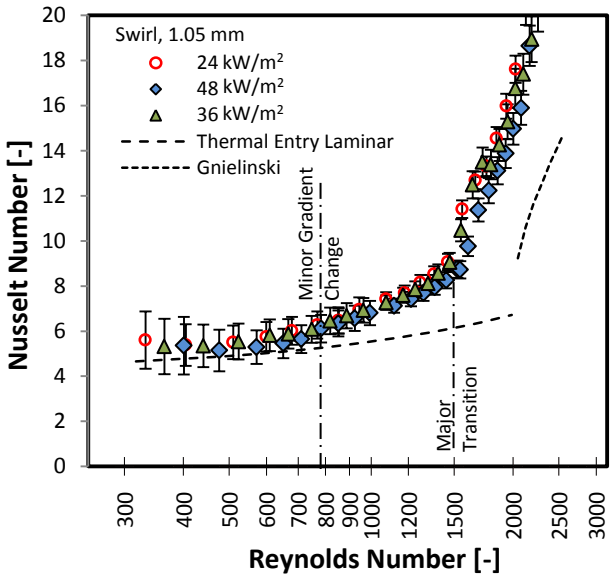

Figure 14 Nusselt numbers with a swirl inlet section for the 1.05 mm test section at different wetted surface heat fluxes

testing was limited to maximum Reynolds number of 2 300. However, it was still possible to observe the transition within this limited Reynolds number range.

The Shah and London correlation was in good agreement with the friction factors at Reynolds numbers below 800. The effect of a decreasing friction factor due to an increase in the heat flux was also observed with this inlet type, even in the transition flow regime. At a Reynolds number of approximately 800, the gradient of the friction factor trend changed and measured friction factors started to differ from the Shah and London predictions. In this region the Shah and London correlation under-predicted the friction factor by an average of 12%. An early transition regime began at a Reynolds number of approximately 1 500 and ended shortly thereafter at a Reynolds number of approximately 1 700. The friction factor results and the Blasius equation showed good agreement at a Reynolds numbers between 1 700 and 2 300. It must, however, be noted that the gradient of the friction factor trend seems to be different from that of the Blasius equation which may indicate that full transition was not over yet.

As expected, the average Nusselt numbers obtained with the swirl inlet type were found to be higher than the Nusselt numbers observed with the sudden contraction and bellmouth inlets. The Laminar regime Nusselt number increased steadily, and as with the friction factor results exhibited a gradient

change at a Reynolds number of 800 until major transition occurred at a Reynolds number of approximately 1 500 (similar as with the friction factor). For Reynolds numbers above 1 700 the Nusselt number was under-predicted by the Gnielinski equation by approximately 25%.

4.3 Comparison of results

4.3.1 Critical Reynolds numbers

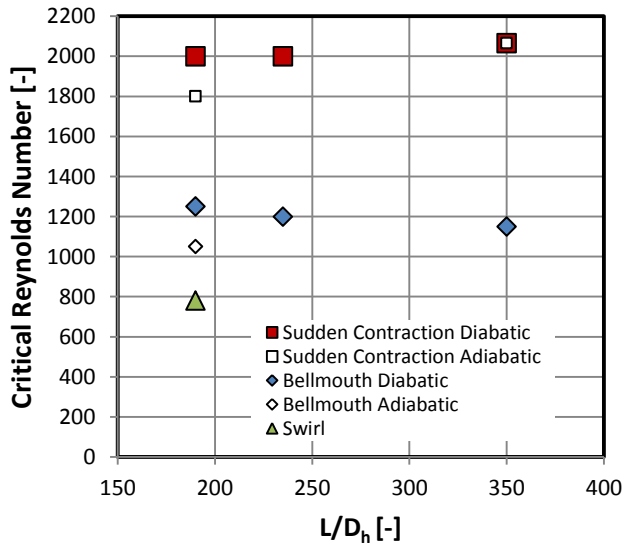

Figure 15 Summary of critical Reynolds numbers in terms of the length to diameter ratio

Figure 15 gives a summary of the critical Reynolds numbers as obtained for the different inlet types and channel diameters in terms of the length to diameter ratio L/D_h. The critical Reynolds numbers were determined according to when the first observable deviation in either the friction factor or Nusselt number results was noticed. For the Bellmouth inlet type these correspond to the transitions as indicated in Figures 8, 11 and 12, while for the Swirl inlet type it corresponds to initial gradient change as are indicated in Figures 13 and 14. Because little difference was observed among the critical Reynolds numbers at different heat fluxes, these were grouped together and are indicated as being the diabatic critical Reynolds number for each diameter and inlet type combination. The adiabatic critical Reynolds numbers are included in Figure 15 where it is available. It can be seen that for a given inlet type, L/D_h had a relatively weak influence and that the inlet type seems to have a dominant effect. Earliest transition commenced for the swirl inlet at about Re = 800, followed by the

Bellmouth inlet type at about Re = 1 200 with the sudden contraction inlet type demonstrating transition at about Re = 2 000.

4.3.2 Friction factors

The results of the bellmouth and swirl inlets are compared with the results of the sudden contraction inlet in Table 7 for Reynolds numbers between 800 and 2 000. This Reynolds number range was selected since it covers the transitional regions observed within this study. For the bellmouth inlet, friction factors were comparable with those of the sudden contraction inlet in the laminar regime, but were increased by up to 41% for Reynolds numbers above 1 250 in the 1.05 mm channel, by up to 20% for Reynolds numbers above 1 200 in the 0.85 mm channel, and by up to 32% for Reynolds numbers above 1 150 in the 0.57 mm channel. For the swirl inlet case, the friction factors were increased by between 22% and 77%.

Table 7 Comparison of the bellmouth and swirl inlet section results to the sudden contraction inlet section results for Reynolds numbers between 800 and 2 000

Hydraulic diameter	Inlet	Friction factor increase	Nusselt number enhancement	Notes
1.05 mm	Bellmouth	0% – 41%	0% – 85%	Enhancement for Reynolds numbers above 1 250
	Swirl	22% – 77%	31% – 149%	Enhancement for all Reynolds numbers
0.85 mm	Bellmouth	10% – 20%	11% – 31%	Major enhancement for Reynolds numbers above 1 200
0.57 mm	Bellmouth	2% – 32%	0% – 59%	Enhancement for Reynolds numbers above 1 150

4.3.3 Nusselt numbers

The inlet sections not only influenced the pressure drop along the length of the channel, but also influences the heat transfer coefficients, due to an altered flow profile. As with the friction factor

results, significant differences were also noted in the results of the Nusselt numbers as are contained in Table 7. The Nusselt numbers of the sudden contraction and bellmouth inlet cases were comparable (within 2%) in the laminar flow regime. For the bellmouth inlet, results deviated from the trends of the sudden contraction once the early transition regime was encountered. The bellmouth inlet cases showed increased Nusselt numbers by up to 85%, 31% and 59% for the 1.05 mm, 0.85 mm and 0.57 mm channels respectively. It should be noticed that these increases were more than the increases of the friction factors for the same Reynolds number range. Above Reynolds numbers of approximately 2 300, sudden contraction and bellmouth results were again comparable.

Swirl inlet Nusselt numbers were found to be higher across the whole Reynolds number range. Due to the swirl effect, and an altered flow pattern, better fluid mixing was anticipated which increased the heat transfer coefficient. The results showed an increase in the Nusselt number of between 31% and 149% when compared with the results of the sudden contraction inlet. Again the Nusselt number was increased by a larger margin than the friction factor.

4.4 Colburn j-factor

The Colburn *j*-factor provides a way of representing the Nusselt number by taking into consideration the varying Prandtl number as are defined in equation (18).

$$j = \frac{\overline{Nu}}{RePr^{\frac{1}{3}}} \tag{18}$$

Because the Colburn *j*-factor is related to the Nusselt number, it also showed the effects of the inlet flow conditions. Figure 16 gives the results of the Colburn *j*-factor for the 1.05 mm channel for all the inlet types and wetted channel surface heat flux cases. As with the friction factor and Nusselt number results, the *j*-factor captures the onset of transition of all the inlet types as are indicated by the markers in Figure 16. The swirl inlet *j* factors were higher throughout the experimental range. For Reynolds numbers above 2 000, it was found that the j-factors did not converge and that the *j*-factors for the Bellmouth inlet was higher than for the sudden contraction inlet type, and those for the swirl inlet were even higher.

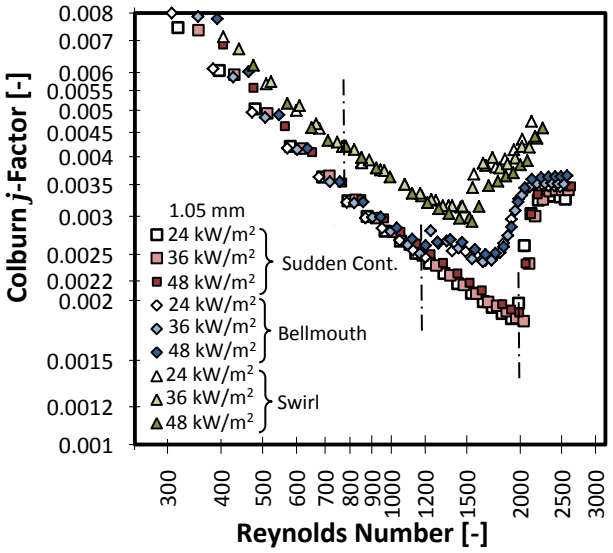

Figure 16 Colburn *j*-factor results for the 1.05 mm test section for different inlet types and heat fluxes

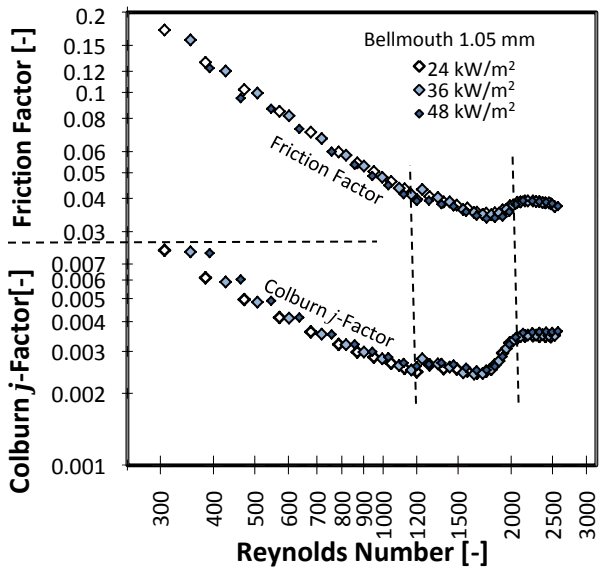

Figure 17 Comparison of the 1.05 mm friction factor and Colburn *j*-factors for a Bellmouth inlet type

Figure 17 plots the *j*-factors and friction factors for the 1.05 mm test section with the sudden contraction inlet type. It can be seen that relatively the same data-profile is present between the *j*-factors and the friction factors. Similar relations were observed for all other test section results. By relating the *j*-factor and friction factor, it is possible to link them to each other. Due to the small size hydraulic diameters of small scale channels, it may not be possible to insert pressure ports directly into the channel as was the case in this study. Pressure drop and friction factors can also be determined with other methods such as the cutting method, however, here it was attempted to develop

a relationship that uses the measured Nusselt number to estimate the friction factor. Using the measurements for all the test sections, the relationship between the friction factor and the Colburn *j*-factor was developed, given in equation 19. Since the relationship requires a measured entity, the friction factor or the Nusselt number (Colburn *j*-factor), the effect of the inlet condition is inherently demonstrated with the input measurements.

$$f_{pred} = \exp\left(\ln(j_{meas})\left(\ln\left(\frac{\ln(Re)}{a} + b\right)\right)\right) \tag{19}$$

$$500 \leq Re \leq 2500$$

$$5 \leq Pr \leq 8$$

$$24\ \mathrm{kW/m^2} \leq \bar{\dot{Q}}''_{wetted} \leq 48\ \mathrm{kW/m^2}$$

$$190 \leq \frac{L}{D_h} \leq 350$$

For the sudden contraction inlet type, $a = 6.53$ and , $b = 0.6$ resulted in 94% of all data points being predicted within 10% of the measured values. For the bellmouth inlet type $a = 7.15$ and , $b = 0.7$ resulted in 94% of all data points being predicted within 10% of the measured values. While for the swirl inlet, $a = 6.64$ and, $b = 0.6$ resulted in 100% of all data points being predicted within 10% of the measured values. Two examples of the accuracy of the relationship are given in Figure 18, for arbitrary chosen sub data-sets, one for the 1.05 mm sudden contraction and one for the 0.57 mm Bellmouth. It can be seen that there is good correlation between the measurements and the predictions across the entire range of the Reynolds number considered in this study. Figure 19 demonstrates the accuracy of all data points captured at different channel diameters, inlet types and wetted surface heat flus levels. It can clearly be seen that almost all data points were predicted within ±10% of the measurements.

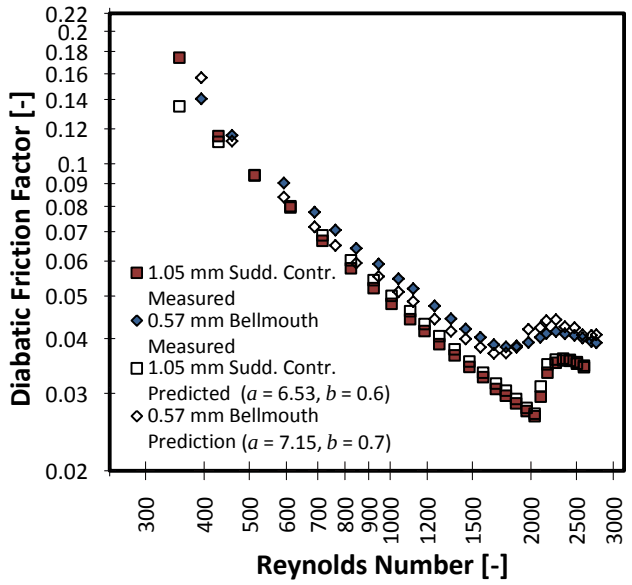

Figure 18 Comparison of predicted friction factors and measured friction factors for two arbitrary chosen sub data-sets.

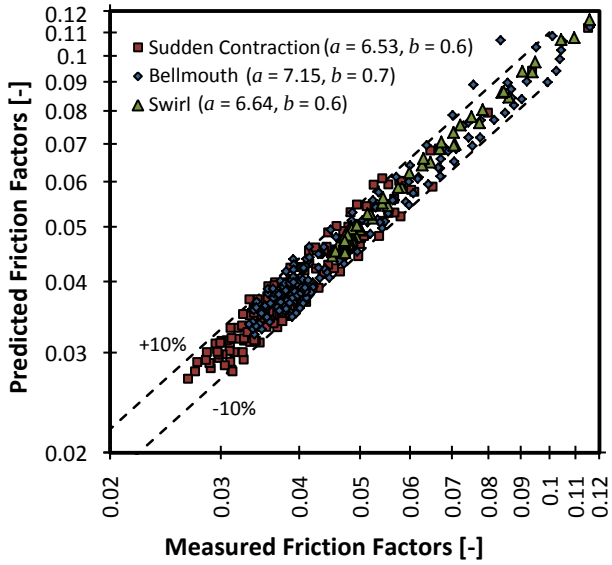

Figure 19 Predicted friction factors versus measured friction factors for all data

5 Conclusions

The effect of inlet flow conditions on the friction factor and the heat transfer coefficient was investigated in this study for small scale rectangular channels having hydraulic diameters of 0.57 mm, 0.85 mm, and 1.05 mm. The laminar and transition regimes were investigated with sudden contraction, bellmouth and swirl inlet sections. It was found that the inlet configuration had a

definite influence on especially the transition flow regime. The swirl inlet type was found to alter the Nusselt number and friction factor behaviour in all of the flow regimes.

Adiabatic laminar friction factors were predicted well by the Shah and London, but were over-predicted by up to 15% during diabatic test runs. A decrease in friction factor was observed with an increase in heat input due to a reduction in the fluid viscosity at the wall. Correcting for the friction factor using the viscosity ratio in the laminar regime improved on the accuracy, but due to the correction method being dependent on the flow field, this needs further investigation. In general friction factors for Reynolds numbers above 2 300 were over-predicted by the Blasius equation expect for the swirl inlet type.

For the sudden contraction inlet type adiabatic transition commenced at a Reynolds number of 1 800 while diabatic transition only commenced at a Reynolds number of 2 000. Transition for the bellmouth inlet type was much smoother than the abrupt transition observed with the sudden contraction inlet, and lasted for a longer Reynolds number range. For the bellmouth inlet type adiabatic transition commenced at a Reynolds number of about 1 050 while diabatic transition commenced at a Reynolds number of about 1 200. The length to diameter ratio only had a minor influence on the critical Reynolds number. For the swirl inlet type a major transition occurred at a Reynolds number of 1 600, but a minor adjustment of the flow condition was also observed at a Reynolds number of 800.

Laminar regime Nusselt numbers were in relative good agreement with the thermal entry length Nusselt number model for macro-scale channels. In general, Nusselt numbers for Reynolds numbers above 2300 were under-predicted by the Gnielinski correlation. In the laminar regime the sudden contraction inlet and bellmouth inlets exhibited similar Nusselt numbers and friction factors, while the Bellmouth inlet type produced higher Nusselt numbers and friction factors in its transition compared to the sudden contraction inlet. Nusselt numbers and friction factors for the swirl inlet type were higher than that of both the sudden contraction and bellmouth inlet probably due to better fluid mixing. The effects of inlets have been proven significant, and can be used to induce greater heat

transfer rates in different regimes, such as using the bellmouth inlet to increase the heat transfer rate. It could also explain to some extent why other studies delivered conflicting results. A set of relationships was derived for the three inlet types to estimate the friction factor using the measured Nusselt number. The relationships predicted between 94% and 100% of the diabatic friction factors within 10% of the measured values, depending on the inlet type.

Aspects that could be considered for investigation in further work include:

- The influence of other inlet configurations.
- Buyancy effects that can result in secondary flow and which can impact on heat transfer and pressure drop.
- The relationship between diabatic and adiabatic friction factors for different flow configuration in developing flow.

References

[1] D.B. Tuckerman and R.F.W. Pease, High-performance heat sinking for VLSI, IEEE Electron Device Letters, EDL-2 (5) (1981) 126 – 129.

[2] X.F. Peng and G.P. Peterson, Convective heat transfer and flow friction for water flow in microchannel structures, International Journal of Heat and Mass Transfer, 39(12) (1996) 2599 – 2608.

[3] G.M. Mala and D. Li, Flow characteristics of water in microtubes, International Journal of Heat and Fluid Flow, 20 (1999) 142 – 148.

[4] T.M. Harms, M.J. Kazmierczak and F.M. Gerner, Developing convective heat transfer in deep rectangular microchannels, International Journal of Heat and Fluid Flow, 20 (1999) 149 – 157.

[5] Q. Weilin, G.M Mala and L. Dongqing, Pressure-driven water flows in trapezoidal silicon microchannels, International Journal of Heat and Mass Transfer, 43 (2000) 353 – 364.

[6] J. Judy, D. Maynes and B.W. Webb, Characterization of frictional pressure drop for liquid flows through microchannels, International Journal of Heat and Mass Transfer, 45 (17) (2002) 3477 – 3489.

[7] H.E. Hegab, A. Bari and T.A. Ameel, Friction and convection studies of R-134a in microchannels within the transition and turbulent flow regimes, Journal of Experimental Heat Transfer, 15 (4) (2002) 245 – 259.

[8] G.P. Celata, M. Cumo and G. Zummo, Thermal-hydraulic characterisatics of single-phase flow in capillary tubes, Experimental Thermal and Fluid Science, 28 (2-3) (2004) 87 – 95.

[9] S.V. Garimella and V. Singhal, Single-phase flow and heat transport and pumping considerations in microchannel heat sinks, Heat Transfer Engineering, 25 (1) (2004) 15 – 25.

[10] P.F. Hao, F. He and K.Q. Zhu, Flow characteristics in a trapezoidal silicon microchannel, Journal of Micromechanics and Microengineering, 15 (2005) 1362 – 1368.

[11] M.E. Steinke and S.G. Kandlikar, Single-phase liquid friction factors in microchannels, International Journal of Thermal Sciences, 45 (11) (2006) 1073 – 1083.

[12] P. Hrnjak and X. Tu, Single-phase pressure drop in microchannels, International Journal of Heat and Fluid Flow, 28 (2007) 2 – 14.

[13] Celata G.P., M. Lorenzini, G. Morini and Z. G., Friction factor in micropipe gas flow under laminar, transition and turbulent flow regime, International Journal of Heat and Fluid Flow, 30 (2009) 814 – 822.

[14] V.K. Natrajan and K.T. Christensen, Non-intrusive measurements of convective heat transfer in smooth- and rough-wall microchannels: laminar flow, Journal of Experimental Fluids, 49 (5) (2010) 1021 – 1037.

[15] G.L. Morini, M. Lorenzini, S. Salvigni and G.P. Celata, Experimental analysis of microconvective heat transfer in the laminar and transitional regions, Experimental Heat Transfer, 23 (1) (2010) 73 – 93.

[16] A. Ghajar, C. Tang and W. Cook, Experimental investigation of friction factor in the transition region for water flow in minitubes and microtubes, Heat Transfer Engineering, 31 (8) (2010) 646 – 657.

[17] Tam, H. K., Tam, L. M., Ghajar, A. J., Ng, W. S., Wong, I. W., Leong, K. F., and Wu, C. K., The Effect of Inner Surface Roughness and Heating on Friction Factor in Horizontal Micro-Tubes, Proceedings of ASME-JSME-KSME Joint Fluids Engineering Conference 2011(AJK2011 FED), Hamamatsu, Shizuoka, Japan, July 24 – 29, 2011.

[18] L. Tam, H. Tam and A. Ghajar, Heat Transfer Measurements for a Horizontal Micro-Tube Using Liquid Crystal Thermography, Proceedings of ISHTEC2012, the 4th International Symposium on Heat Transfer and Energy Conservation, Paper no. TC02 007, Guangzhou, China, 2012.

[19] R. Bavière, M. Favre-Marinet and S. Le Person, Bias effects on heat transfer measurements in microchannel flows, International Journal of Heat and Mass Transfer, 49 (2006) 3325 – 3337.

[20] H. Herwig and O.Hausner, Critical view on "new results in micro-fluid mechanics": an example, International Journal of Heat and Mass Transfer, 46 (2003) 935 – 937.

[21] G. Maranzana, I. Perry and D. Maillet, Mini- and micro-channels: influence of axial conduction in the walls, International Journal of Heat and Mass Transfer, 47 (17 – 18) (2004) 3993 – 4004.

[22] R. Chein and J. Chen, Numerical study of the inlet/outlet arrangement effect on microchannel heat sink performance, International Journal of Thermal Sciences, 48 (2009) 1627 – 1638.

[23] B. Palm, Heat transfer in microchannels, Microscale Thermophysical Engineering, 5 (2001) 155 – 174.

[24] Z.-Y. Guo and Z.-X. Li, Size effect on microscale single-phase flow and heat transfer, International Journal of Heat and Mass Transfer, 46 (2003) 149 – 159.

[25] A. J. Ghajar and K.F. Madon, Pressure drop measurements in the transition region for a circular tube with three different inlet configurations, Experimental Thermal and Fluid Science, 5 (1) (1992) 129 – 53.

[26] A. J. Ghajar and L.M. Tam, Heat transfer measurements and correlations in the transition region for a circular tube with three different inlet configurations, Experimental Thermal and Fluid Science, 8 (1) (1994) 79 – 90.

[27] L.M Tam and A.J. Ghajar, Effect of inlet geometry and heating on the fully developed friction factor in the transition regime of a horizontal tube, Experimental Thermal and Fluid Science, 15 (1) (1997) 52 – 64.

[28] L.M Tam and A.J. Ghajar, The unusual behavior of local heat transfer coefficient in a circular tube with a bell-mouth inlet, Experimental Thermal and Fluid Science, 16 (3) (1998) 187 – 194.

[29] L.M Tam and A.J. Ghajar, Transitional heat transfer in plain horizontal tubes, Heat Transfer Engineering, 27 (5) (2006) 23 – 38.

[30] H.K. Tam, L. M Tam , and A. J. Ghajar, Effect of inlet geometries and heating on the entrance and fully-developed friction factors in the laminar and transition regions of a horizontal tube, Experimental Thermal and Fluid Science, 44 (2013) 680 – 696.

[31] J.A. Olivier and J.P. Meyer, Single-phase heat transfer and pressure drop of the cooling of water inside smooth tubes for transitional flow with different inlet geometries (RP-1280), HVAC&R Journal, 16 (4) (2010) 471 – 496.

[32] J.P. Meyer and J.A. Olivier, Transitional flow inside enhanced tubes for fully developed and developing flow with different types of inlet disturbances: Part I – adiabatic pressure drop, International Journal for Heat and Mass Transfer, 54 (7 – 8) (2011) 1587 – 1597.

[33] J.P. Meyer and J.A. Olivier, Transitional flow inside enhanced tubes for fully developed and developing flow with different types of inlet disturbances: Part II – heat transfer, International Journal for Heat and Mass Transfer, 54 (7 – 8) (2011) 1598 – 1607.

[34] J.P. Meyer, T.J. McKrell, and K. Grote, The influence of carbon nanotubes on single-phase heat transfer and pressure drop characteristics in the transitional flow regime of smooth tubes, International Journal of Heat and Mass Transfer, 58 (1 – 2) (2130) 597 – 609.

[35] T. Morel, Comprehensive design of axisymmetric wind tunnel contractions, Journal of Fluids Engineering, 97 (1975) 225 – 233.

[36] O. Aydin and M. Baki, An experimental study on the design parameters of a counterflow vortex tube, Energy, 31 (14) (2006) 2763 – 2772.

[37] C.O. Popiel and J. Wojtkowiak, Simple formulas for thermophysical properties of liquid water for heat transfer calculations (from 0°C to 150°C), Heat Transfer Engineering, 19 (3) (1998) 87 – 101.

[38] V. Gnielinski, New equations for heat and mass transfer in turbulent pipe and channel flow, International Chemical Engineering, 16 (2) (1976) 359 – 367.

[39] R.K. Shah and A.L. London, Laminar flow forced convection in ducts, Academic Press, New York, 1978, pp. 196 – 222.

[40] Y.S. Muzychka and M. M. Yovanovich, Pressure drop in laminar developing flow in noncircular ducts: A scaling and modeling approach, Journal of Fluids Engineering, 131 (2009), Article number 111105, 1 – 11.

[41] S. Kakaç, R.K. Shah and W. Aung, Handbook of single-phase heat transfer, Whiley interscience, New York, 1987, Chapter 18, pp. 18.1 – 18.8

[42] R. Moffat, Describing the uncertainties in experimental results, Experimental Thermal and Fluid Science, 1 (1988) 3 – 17.

[43] Y.A. Céngel, Heat Transfer: A Practical Approach 2nd Edition, second (SI) ed., McGraw-Hill, New York, 2004, pp. 419 – 458.